Proceedings of the Thirty-second (2022) International Ocean and Polar Engineering Conference **www.isope.org**
Shanghai, China, June 5–10, 2022

ISBN 978-1-880653-81-4; ISSN 1098-6189

Numerical Analysis of Vortex-Induced Vibration Suppression of a Flexible Riser Attaching with Symmetric Strips

*Hao Hu[1], Zhiyuan Wei[2], Decheng Wan[1]**

[1]Computational Marine Hydrodynamic Lab (CMHL), School of Naval Architecture, Ocean and Civil Engineering, Shanghai Jiao Tong University, Shanghai, China
[2]Marine Design and Research Institute of China, Shanghai, China
*Corresponding author

ABSTRACT

A computational fluid dynamics (CFD) model is built to analyze the Vortex-Induced Vibration (VIV) Suppression of a flexible riser attaching with symmetric strips suffering to the uniform current. The thick strip model and the Navier-Stokes method are applied to solve the flow field, the Bernoulli–Euler bending beam model and Finite Element Method (FEM) are employed to obtain the vibration displacements of riser. During numerical calculations, the symmetric strips are arranged at 45 degree on the surface of riser to the flow direction with a constant width of 0.2D and three varying thicknesses of 0.03D, 0.05D and 0.08D. The dimensionless Root Mean Square (RMS) displacements, modal weights, vibration frequencies, and the wake flow field are compared. The results indicate that this configuration has fine ability to suppress VIV especially at the symmetric strips thickness of 0.08D.

KEY WORDS: VIV suppression; uniform current; symmetric strips; viv3D-FOAM-SJTU solver;

INTRODUCTION

The positive and negative vortices are released in the wake region of the marine riser when it suffers to current. The generation and migration of these vortices bring a typical fluid-structure interaction phenomenon called VIV. Due to the large aspect ratio of the marine riser, the huge deflection of the marine riser caused by VIV contributes to the fatigue damage, which results in the leakage of internal gas and oil. Therefore, to ensure the stability of the marine riser, the VIV control strategies have been researched by many scholars in the past decades.

Hong and Shah (2018) had reviewed the recent investigations on the passive and active control strategies of VIV. Considering maintenance and economical costs, the marine riser is commonly equipped with the passive control devices. Thus, the researches on the passive control methods are introduced in the following subsection.

Huera-Huarte (2017) tested the VIV of the cylinder with different densities and sizes wire meshes, they concluded that this device can affect the boundary layer and suppress the vortex street, meanwhile, the drag coefficient had no increased in most cases. Ren et al (2019) experimentally investigated the VIV suppression effect of the flexible riser with different Keulegan-Carpenter (KC) numbers and maximum reduced velocities in oscillatory flow, the analysis results indicated that the suppression efficiency in oscillatory flow was limited at low KC numbers and reduced velocities compared to uniform flow. Li et al (2020) conducted an experiment to verify the VIV suppression effect of the flexible cylinder installing with the bird-wing-shaped device, the results showed that the velocity of flow field was reduced, and the VIV suppression effect was related to the length of device. Li et al (2020) experimentally studied the VIV responses of the discrete helical strake flexible riser with different start helical strakes and discrete spacings, and they found that the three-starts discrete helical strakes showed the best suppression effect regardless of different discrete spacings.

Law and Jaiman (2018) modified the rigid cylinder with staggered and helical grooves, the numerical simulations showed that the rigid cylinder with staggered grooves showed more high suppression efficiency, where the inline and crossflow amplitudes were reduced to 37% and 75% respectively. Zhu (2020) developed two-dimensional numerical model with direct numerical simulation (DNS) to investigate the VIV suppression efficiency of a cylinder with splitter plates located upstream and downstream, this arrangement can effectively suppress VIV at certain reduced velocity, and the suppression efficiency was improved with the longer plate. Ishihara and Li (2020) constructed the CFD model through Large eddy simulation (LES) turbulence method to simulate the VIV responses of the rigid cylinder with helical wires, it was found in the numerical results that the lift coefficient was

suppressed with no enhancement of drag coefficients. Wang (2020) numerically investigated the VIV of the rigid cylinders with modified surface referring to the giant cactus, and they found that the crossflow and inline amplitudes were both decreased as the increment of height of the bionic structure.

In conclusion, many experimental and numerical investigations on the VIV suppression have been done. However, the previous numerical studies mostly focused on the VIV suppression of two-dimensional and three-dimensional rigid cylinder, the numerical computations on VIV suppression of the three-dimensional slender flexible cylinder were limited. In this paper, the flexible riser attaching with symmetric strips of three different depths at a certain angle is select to investigate the VIV suppression effect, which is proved an effective method for the rigid cylinder referring to the Ma et al (2021). The whole simulations are carried out by viv3D-FOAM-SJTU solver developed on the thick strip model and OpenFOAM, which has been validated by Deng et al (2020). The remaining article is organized as follows: Section II introduces the numerical method dealing with fluid-structure interaction. Section III describes the numerical setup and boundary conditions. Section IV gives the introduction to the discussion of the simulation results. Section V presents the brief conclusion for the paper.

NUMERICAL METHOD

Hydrodynamic governing equations

In order to obtain the hydrodynamic force acting on the flexible riser, the Navier-Stokes equations for the incompressible viscous flow are applied, and the continuity and momentum equations are shown as follows:

$$\frac{\partial \overline{u_i}}{\partial x_i} = 0, \tag{1}$$

$$\frac{\partial u_i}{\partial t} + \frac{\partial u_i u_j}{\partial x_j} = -\frac{1}{\rho}\frac{\partial p}{\partial x_i} + \frac{\partial}{\partial x_j}\left[\nu\left(\frac{\partial u_i}{\partial x_j} + \frac{\partial u_j}{\partial x_i}\right)\right]. \tag{2}$$

Here, ρ represents the density of incompressible fluid, p represents the pressure, ν represents kinematic viscosity of the fluid, and i, j =1, 2, 3 represent components of physical quantity in Cartesian coordinate system.

Considering the small-scale vortex structure released by VIV of the complex cross-section of flexible riser, the shear stress transport (SST) k-ω turbulence model and delayed detached-eddy simulation (DDES) model, which briefly called SST-DDES model, are coupled to resolve the momentum equation. This hybrid RANS-LES method (SST-DDES model) decomposes the whole flow field into the near-wall region solved by RANS method and separated flow region solved by LES method. Meanwhile, the blending length l_{DES} is applied to switch the RANS computation region to the LES computation region. Therefore, the modified transport equations for turbulence kinetic energy k and turbulence dissipation rate ω can be rewritten as:

$$\frac{\partial k}{\partial t} + \frac{\partial (u_j k)}{\partial x_j} = G - \frac{k^{3/2}}{l_{DES}} + \frac{\partial}{\partial x_j}\left[\left(\nu + \alpha_k \nu_t\right)\frac{\partial k}{\partial x_j}\right], \tag{3}$$

$$\frac{\partial \omega}{\partial t} + \frac{\partial \left(u_j \omega\right)}{\partial x_j} = \gamma S^2 - \beta\omega^2 + \frac{\partial}{\partial x_j}\left[\left(\nu + \alpha_\omega \nu_t\right)\frac{\partial \omega}{\partial x_j}\right] + 2\left(1 - F_1\right)\frac{\alpha_{\omega 2}}{\omega}\frac{\partial k}{\partial x_j}\frac{\partial \omega}{\partial x_j}. \tag{4}$$

Here, $\tilde{G} = \min\left(\nu_t S^2, c_1 \beta^* k\omega\right)$, in which the ν_t is the turbulent eddy viscosity, S is the invariant measure of the strain rate, F_1 is the blending function, the values for α_k, γ, β, α_ω, $\alpha_{\omega 2}$, c_1, β^* are fixed (Zhao and Wan, 2016).

Structural governing equations

The Bernoulli–Euler bending beam model is applied to obtain the inline and crossflow vibration displacements of the flexible riser. Therefore, the governing equations for each discrete structural element in x (inline) and y (crossflow) directions are given following:

$$EI\frac{\partial^4}{\partial z^4}x(z,t) - \frac{\partial}{\partial z}\left[T(Z)\frac{\partial x(z,t)}{\partial z}\right] + m\frac{\partial^2 x(z,t)}{\partial t^2} + c\frac{\partial x(z,t)}{\partial t} = f_x(z,t), \tag{5}$$

$$EI\frac{\partial^4}{\partial z^4}y(z,t) - \frac{\partial}{\partial z}\left[T(Z)\frac{\partial y(z,t)}{\partial z}\right] + m\frac{\partial^2 y(z,t)}{\partial t^2} + c\frac{\partial y(z,t)}{\partial t} = f_y(z,t). \tag{6}$$

Here, EI is the bending stiffness, $T(Z)$ is the axial tension along the span of riser, m is the element mass, c is the damping, $f(z,t)$ is hydrodynamic forces acting on the surface of riser.

Then, the governing equations for the whole element of riser based on the FEM have following forms:

$$\mathbf{M}\ddot{\mathbf{x}} + \mathbf{C}\dot{\mathbf{x}} + \mathbf{K}\mathbf{x} = \mathbf{F_{HX}}, \tag{7}$$

$$\mathbf{M}\ddot{\mathbf{y}} + \mathbf{C}\dot{\mathbf{y}} + \mathbf{K}\mathbf{y} = \mathbf{F_{HY}}. \tag{8}$$

Here, **M, C** and **K** are the mass, the damping and the stiffness matrices respectively, $\mathbf{F_H}$ is hydrodynamic force vectors. Meanwhile, the Rayleigh model (Duanmu et al, 2018) is used to calculate the damping matrix instead of the practical damping.

Thick strip model

The strip theory has been proved to be effective in the numerical calculation of the surrounding flow flied of the slender flexible riser (Duanmu et al, 2018; Fu et al, 2018). However, with no consideration of the axial correlation in the three-dimensional flow field, the traditional two-dimensional uniformly fluid strips along the span of flexible riser cannot obtain the accurate hydrodynamic forces acting on the riser attaching with additional structure. Thus, the Bao et al (2016) extends the two-dimensional fluid strips to the three-dimensional fluid strips, and this method is called the generalized thick strip theory (Fig.1). The viv3D-FOAM-SJTU solver is developed based on thick strip model by Deng et al (2020), which has successfully predicted the VIV responses of the flexible riser exposed to uniform flow.

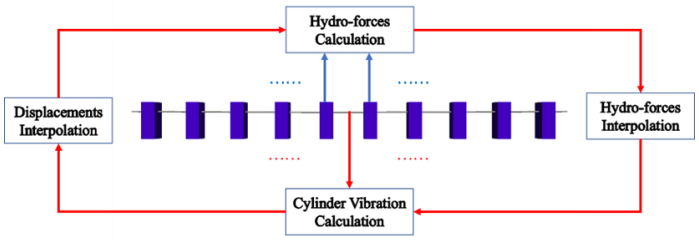

Fig.1 the diagrammatic sketch of the generalized thick strip

In the viv3D-FOAM-SJTU solver, the Iterative calculation for the flow field of each thick fluid strip is PIMPLE algorithm, and the Newmark-β algorithm is employed to solve the displacements of structural vibration in the inline and crossflow directions. Moreover, the hydrodynamic

forces are acted as uniform loads on each structural element through cubic spline interpolation theory. The two-way coupling strategy (Duanmu, 2018) is adopted to handle the fluid-solid interaction of the VIV of riser.

NUMERICAL SETUP

In this paper, the flexible riser referring to the experiments carried out by Lehn (2003) is selected as the research object, and the corresponding simulation results solved by viv3D-FOAM-SJTU solver (Deng et al, 2020) are adopted for detailed comparisons. The symmetric strips with 45 degree to the flow direction are attached to the riser model inspired by the simulations of Ma et al (2021). The details of geometric model for this configuration are illustrated in Fig.2, where α is the angle, w is the width of the strip, and d is the thickness of the strip. In all simulations, the riser is located at the uniform current of 0.2m/s. Three cases (table 1) are simulated with a fixed value of w = 0.02D (diameter), and the three values of d = 0.03D, 0.05D, and 0.08D, respectively. In order to ensure the focus on effects of the variation of the cross-section on the VIV suppression of riser, the variation of main structural parameters with different configurations is neglected. Thus, the main structural parameters of different configurations are the same as that of bare riser, which are displayed in Table 2.

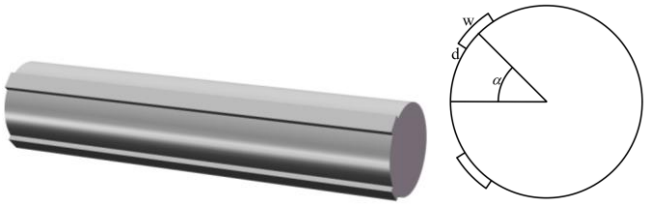

(a) bird view (b) Vertical view

Fig.2 Schematic diagram of geometric model for riser with symmetric strips

Table 1 symmetric strips geometries

	strip width (w)	strip thickness (d)	Unit
Case1	0.2D	0.03D	m
Case2	0.2D	0.05D	m
Case3	0.2D	0.08D	m

Table 2 Main parameters of the riser attaching with symmetric strips

	Properties	Values	Unit
Length	L	9.63	m
Diameter	D	20	mm
Structural stiffness	EI	135.4	N.m^2
Top tension	T	817	N
Mass ratio	m^*	2.23	-
Aspect ratio	L/D	481.5	-
Flow velocity	U	0.2	m/s
First natural frequency	f_{n1}	1.79	HZ
Second natural frequency	f_{n2}	3.67	HZ

As shown in Fig.3(a), the 10 uniform thick fluid strips along the span of riser are the numerical calculation domain for the simulation. Each thick fluid strip domain is set as a $20D\times40D\times1/100L$ cuboid (Fig.3(b)) with about 560000 cells, and Deng et al (2020) has proved that the thickness of $1/100L$ for the fluid strip is required to capture the difference in the axial direction of vortex shedding. It can be seen from Fig.3(c) that the gravity center of the riser attaching with the symmetric strips is set at $10D$ from the distance to the inlet boundary and $10D$ from the distance to the right boundary. The boundary condition for the inlet boundary of each fluid strip is applied with a fixed velocity inlet condition, and the corresponding boundary condition for the outlet boundary of each fluid strip is set as the pressure outlet condition. The boundary conditions for the top, bottom, right and left boundaries are both prescribed as the symmetry conditions. The no-slip boundary condition is employed on each surface of structural element, and the two-ends of the whole riser adopt the simply boundary conditions. The meshes near the surface of each structural element displayed in Fig.3(d-f) are refined with all values of y+ lower than 3 to obtain the accurate values of the pressure and velocity in the viscous sub-layer. The dynamic grid technique called "displacement Laplacian" in the OpenFOAM is used to update the meshes of each fluid strip with the vibrations of riser in the inline and crossflow directions. The slender riser is uniformly decomposed into 200 structural elements. Considering the stability of convergence, the value of the timestep for all simulations is fixed at 0.001s to control the Courant Number lower than 5.0 in the whole process of numerical calculation.

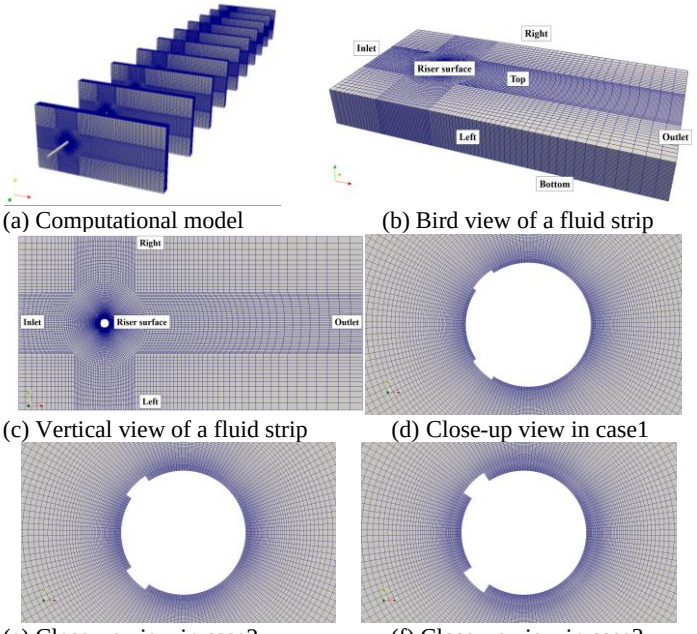

(a) Computational model (b) Bird view of a fluid strip

(c) Vertical view of a fluid strip (d) Close-up view in case1

(e) Close-up view in case2 (f) Close-up view in case3

Fig. 3 Schematic diagram of the computational model

RESULTS AND DISCUSSION

The dimensionless RMS displacements along the span of bare riser (Deng et al, 2020), riser attaching with symmetric strips of different thicknesses (case1, case 2, and case 3) are compared in the crossflow and inline directions (Fig.4). As shown in Fig.4(a), the maximum value of around 0.28D for the dimensionless RMS displacement of the riser with symmetric strips of 0.03D thickness shows the obvious the suppression effect with same vibration shape of the bare riser in the crossflow direction. With the thicknesses of the symmetric strips increasing to 0.05D and 0.08D, although the vibration is close to the second-order shape at 0.05D, the dimensionless RMS displacements continue to decrease with the maximum value of around 0.21D and 0.14D in the crossflow direction respectively. It is can be found in Fig.4(b) that the dimensionless RMS displacements of riser with symmetric strips of different thicknesses share the same suppression effect with little difference maximum values of around 0.064D, 0.071D, 0.070D in the inline direction. The results indicate that the suppression effect of dimensionless RMS displacements in the inline direction are no sensitive to the symmetric strips thickness compared with that in the

crossflow direction. Meanwhile, the dimensionless RMS displacements of riser with symmetric strips of 0.03D and 0.05D thicknesses are close to the first-order vibration shape in the inline direction, which is different from the second-order vibration shape of bare riser.

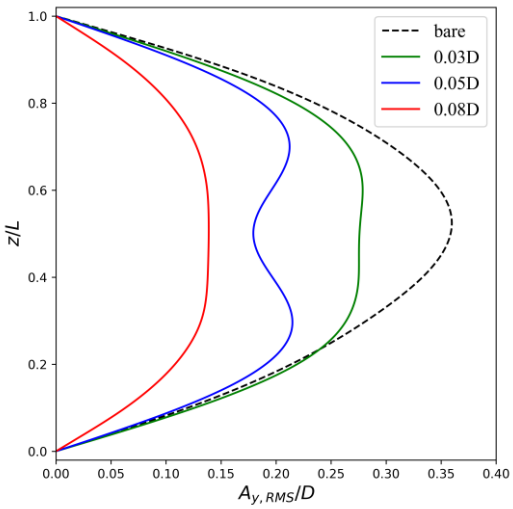

(a)

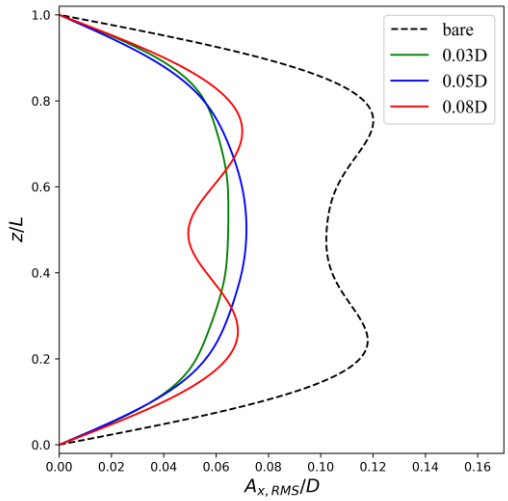

(b)

Fig.4 Comparison of dimensionless RMS of crossflow (a) and inline (b) displacements along the span of riser for bare riser, case 1, case 2 and case 3, respectively.

By applying the modal decomposition and Fast Fourier Transform (FFT) methods, the time-history crossflow vibration modal weights and corresponding PSD of bare riser (Deng et al, 2020), riser attaching with symmetric strips of different thicknesses (case1, case 2, and case 3) are displayed in the Fig.5. Comparing the amplitudes of first-order crossflow mode vibrations, as increasing of the thickness of symmetric strips, it is found that the reduction of amplitudes is continuous, and the wave-type vibrations are more obvious. Meanwhile, the amplitudes of second-order crossflow mode vibrations of all cases are enhanced in comparison with that of bare riser. Thus, the dominant crossflow vibration mode may convert from the first order to second order when the thickness of symmetric strips increases.

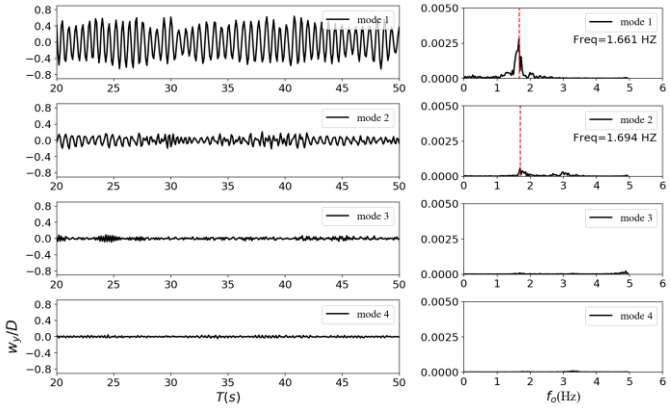

(a) bare riser

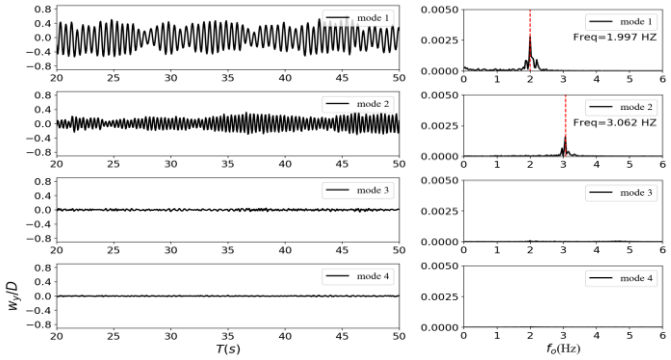

(b) case 1

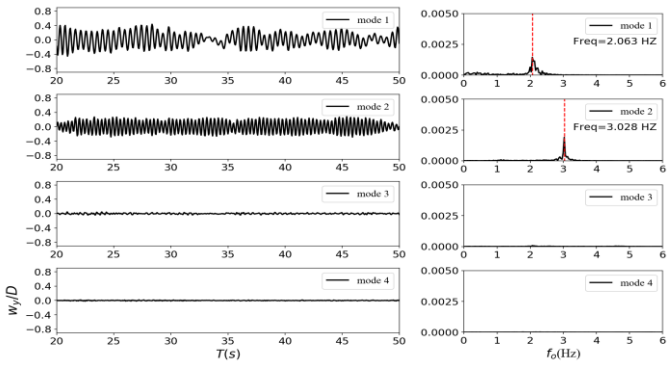

(c) case 2

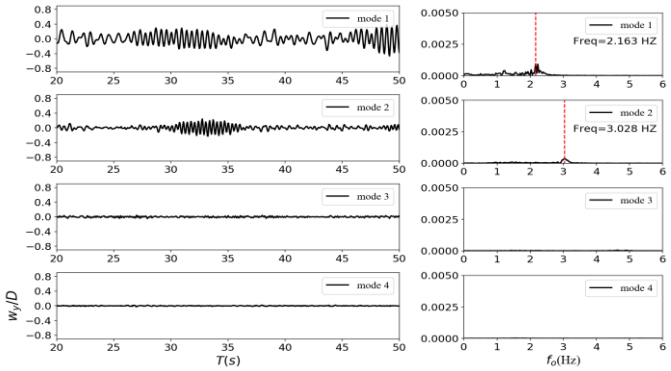

(d) case 3

Fig.5 Time series of crossflow vibration modal weights and corresponding power spectral density (PSD) for bare riser, case 1, case 2 and case 3, respectively.

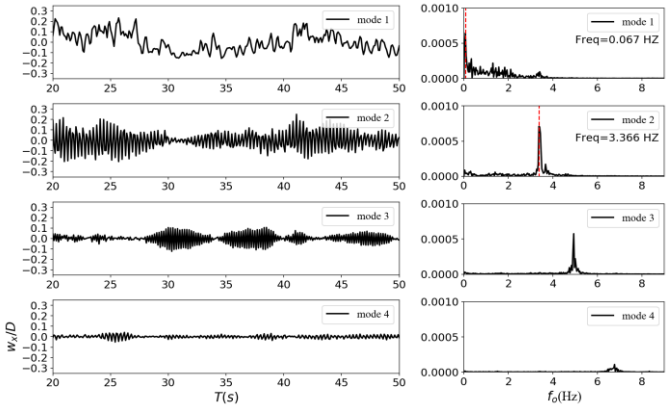

(a) bare riser

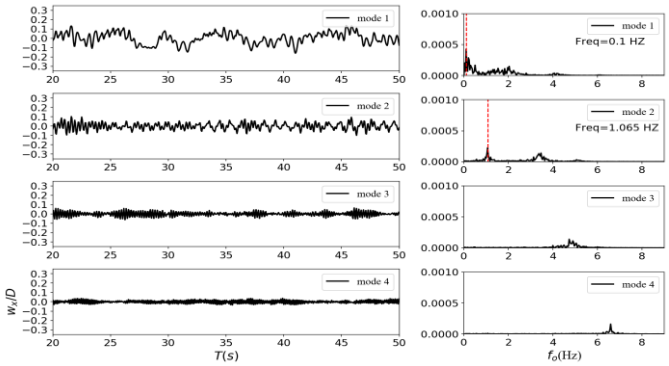

(b) case 1

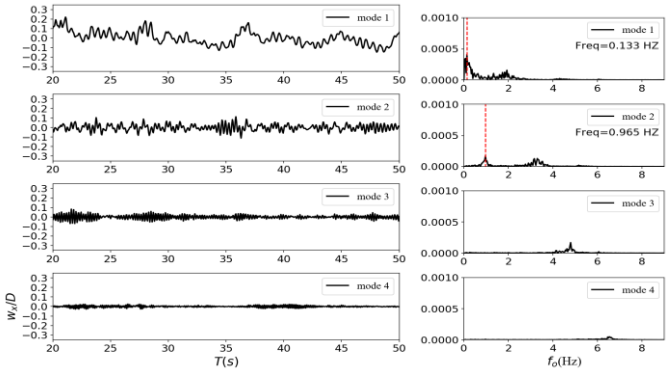

(c) case 2

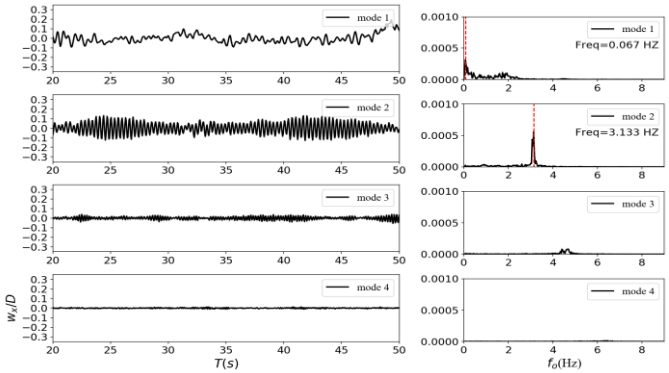

(d) case 3

Fig.6 Time series of inline vibration modal weights and corresponding power spectral density (PSD) for bare riser, case 1, case 2 and case 3, respectively.

As shown in the Figure 5(b-d), compared with that values of 1.661HZ for the bare riser, the values of the crossflow vibration frequencies corresponding to first-order crossflow mode vibrations is 1.997HZ, 2.063HZ, 2.163HZ with increment of symmetric strips thickness, and it is indeed gradually far away from the first-order natural frequency. Meanwhile, the peak of PSD shows a downward trend. Moreover, the crossflow vibration frequencies corresponding to second-order crossflow mode vibrations for all cases are increased, approaching the second-order natural frequency, which induces the increase in the amplitude of the second-order crossflow mode vibration.

The time-history inline vibration modal weights and corresponding PSD of bare riser (Deng et al, 2020), riser attaching with symmetric strips of different thicknesses (case1, case 2, and case 3) are displayed in the Fig.6. It can be seen from Fig.6(b) and (c) that the amplitudes of second-order and third-order inline mode vibrations of riser with symmetric strips of 0.03D and 0.05D thickness show little difference, which are both weaker than bare riser, and the corresponding vibration frequencies for the second-order inline mode vibrations are with the lower values of 1.065 HZ and 0.965HZ, away from the second-order natural frequency. Meanwhile, the corresponding vibration frequencies for the first-order inline mode vibrations are slightly enhanced for case 1 and 2. The above results indicate that the lower frequency inline mode vibration is dominant when the symmetric strips are at the certain thickness. As the symmetric strips thickness reaches to the 0.08D, although the vibration frequency corresponding to second-order inline mode vibration is at a rapprochement with the bare riser, the amplitude of second-order inline mode vibration is still less than that of bare riser.

The Fig.7 shows the instantaneous three-dimensional vortex structures through the Q criterion (Q=5) for the riser attaching with symmetric strips of different thicknesses (case1, case 2, and case 3). As the Fig.7 shown for case 1, 2 and 3, the vortex structures include the wave type, smaller discrete type and regular cylindrical type, which reflect the complex characteristic of three-dimensional vortex shedding. Meanwhile, it is found in the Fig.7 (a) (b) (c) that the different VIV displacements along the span of riser show the different vortices type corresponding to different fluid strips. Moreover, in comparison of the Fig.7 (d), (e) and (h) located at the 5th fluid strip, the vortices of regular cylindrical type are gradually becoming the dominant as the increment of the symmetric strips thickness, however, the variety of the vortices type for the 3rd fluid strip is not obvious with the increase of symmetric strips thickness (Fig.7 (a), (d) and (g)). The above results have proved that the variation of the symmetric strips thickness shows more effect on the vortex structures located at the midspan of riser.

The Fig.8 displays the instantaneous two-dimensional vortex shedding colored by the vorticity-z at the location of z = 5.3m for the riser attaching with symmetric strips of different thicknesses (case1, case 2, and case 3). Unlike the vortex shedding of the bare cylinder, the forced flow separation occurs at the structure of symmetric strips as shown in Fig.8. Compared Fig.8(a), (b) and (c), as the increment of symmetric strips thickness, it is found that the width of vortex street is suppressed. meanwhile, the number of vortices is reduced with increase of symmetric strips thickness. Thus, the reduction of fluid force contributes to the weaken of vibrations.

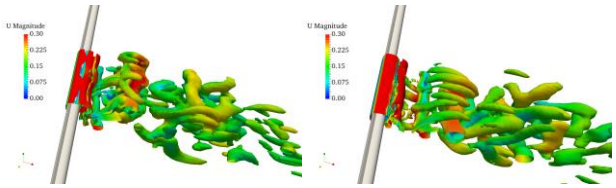

(a) case1, the 3rd strip (b) case1, the 5th strip

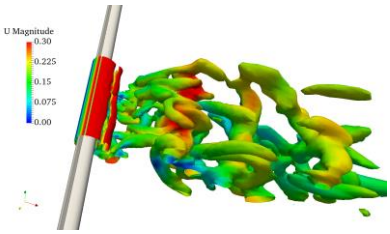

(c) case1, the 7th strip

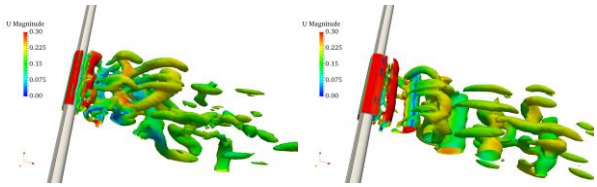

(d) case 2, the 3rd strip (e) case 2, the 5th strip

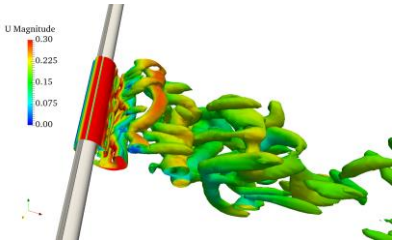

(f) case 2, the 7th strip

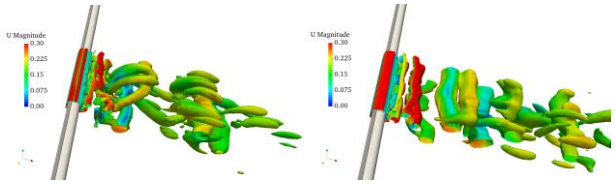

(g) case 3, the 3rd strip (h) case 3, the 5th strip

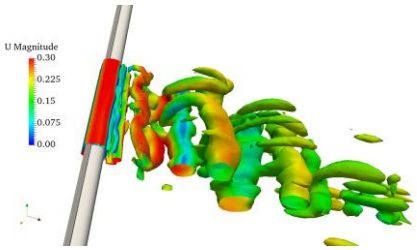

(l) case 3, the 7th strip

Fig.7 Instantaneous vortex structures through the Q criterion (Q=5) of three fluid strips at t=47s for case 1, case 2 and case 3.

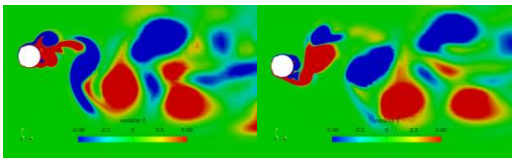

(1) t=46.0s (2) t=46.2s

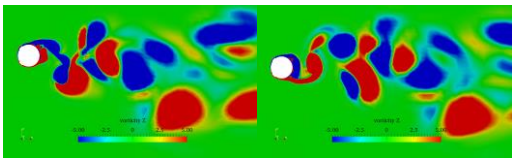

(3) t=46.4s (4) t=46.6s

(a) case 1, z=5.3

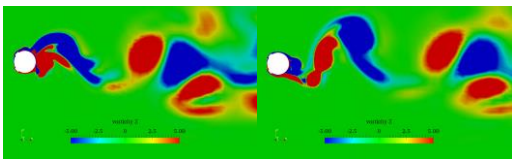

(1) t=46.0s (2) t=46.2s

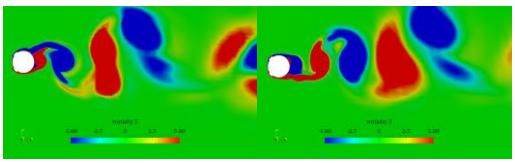

(3) t=46.4s (4) t=46.6s

(b) case 2, z=5.3m

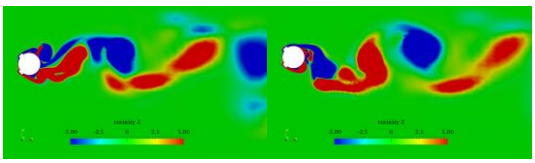

(1) t=46.0s (2) t=46.2s

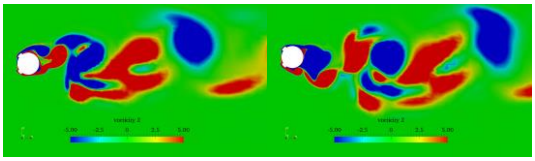

(3) t=46.4s (4) t=46.6s

(c) case 3, z=5.3 m

Fig.8 Instantaneous vorticity-z ($\omega_z = \frac{dv}{dx} - \frac{du}{dy}$) contours at the same axial location along the span of riser for case 1, case 2 and case 3.

CONCLUSIONS

In this paper, the simulations are carried out to investigate the VIV suppression effect of the riser attaching with symmetric strips of a fixed width and three varying thicknesses (0.03D, 0.05D, 0.08D), and the riser exposes to the uniform current with a fixed velocity of 0.2m/s. Through the analysis of the dimensionless RMS displacements, modal

weights, PSD, and the wake flow field, the conclusions are presented that the riser with three thicknesses of symmetric strips all show the suppression effect in the dimensionless RMS displacements with the relative best suppression performance at the 0.08D thickness, and the crossflow and inline vibration frequencies exhibit correlation of variation of symmetric strips thickness. Moreover, the vortex structure is changed and the vortex street is suppressed with the variation of symmetric strips thickness.

ACKNOWLEDGEMENTS

This work was supported by the National Natural Science Foundation of China (51879159, 52131102), and the National Key Research and Development Program of China (2019YFB1704200), to which the authors are most grateful.

REFERENCES

Bao, Y, Palacios, R and Graham, M, et al (2016). "Generalized thick strip modelling for vortex-induced vibration of long flexible cylinders," *J Comput Phys*, 321, 1079–1097.

Deng, D, Zhao, WW, and Wan, DC (2020). "Vortex-induced vibration prediction of a flexible cylinder by three-dimensional strip model," *Ocean Eng*, 205, 107318.

Duanmu, Y, Zou, L, and Wan, DC (2018). "Numerical analysis of multi-modal vibrations of a vertical riser in step currents," *Ocean Eng*, 152, 428-442.

Fu, B, Zou, L, and Wan, DC (2018). "Numerical study of vortex-induced vibrations of a flexible cylinder in an oscillatory flow," *J Fluid Struct*, 77, 170-181.

Huera-Huarte, FJ (2017). "Suppression of vortex-induced vibration in low mass-damping circular cylinders using wire meshes," *Mar Struct*, 55, 200-213.

Hong, K-S, and Shah, UH (2018). "Vortex-induced vibrations and control of marine risers: A review," *Ocean Eng*, 152, 300-315.

Ishihara, TS, and Li, T (2020). "Numerical study on suppression of vortex-induced vibration of circular cylinder by helical wires," *J Wind Eng Ind Aerod*, 197, 104081.

Law, YZ, and Jaiman, RK (2018). "Passive control of vortex-induced vibration by spanwise grooves," *J Fluid Struct*, 83, 1-26.

Lehn, E (2003). "VIV Suppression Tests on High L/D Flexible Cylinders," Norwegian Marine Technology Research Institute, Trondheim, Norway.

Li, P, Liu, LH, and Dong, ZK (2020). "Investigation on the spoiler vibration suppression mechanism of discrete helical strakes of deep-sea riser undergoing vortex-induced vibration," *Int J Mech Sci*, 172, 105410.

Li, ZF, Song, GG, and Chen, YL (2020). "Experimental study on bird-wing-shaped suppression device for vortex-induced vibration of deep water risers," *Ocean Eng*, 213, 107669.

Ma, CH, Zhao, WW, and Wan, DC (2021). "Numerical investigations of three-dimensional flows around a cylinder attaching with symmetric strips," *Phys Fluids*, 33, 075101.

Ren, HJ, Xu, YW, and Cheng, JY, et al (2019). "Vortex-induced vibration of flexible pipe fitted with helical strakes in oscillatory flow," *Ocean Eng*, 189, 106274.

Wang, W, Song, BW, and Mao, ZY (2020). "Numerical investigation on VIV suppression of the cylinder with the bionic surface inspired by giant cactus," *Ocean Eng*, 214, 107775.

Zhao, WW, and Wan, DC (2016). "Numerical study of 3D flow past a circular cylinder at subcritical Reynolds number using SST-DES and SST-URANS," *Chin J Hydrodyn Ser A*, 31, 1-8.

Zhu, HJ, Li, GM, and Wang JL (2020). "Flow-induced vibration of a circular cylinder with splitter plates placed upstream and downstream individually and simultaneously," *Appl Ocean Res*, 97, 102084.